THE JOURNAL OF BIOLOGICAL CHEMISTRY VOL. 287, NO. 22, pp. 18717–18729, May 25, 2012

Impaired Manganese Metabolism Causes Mitotic Misregulation*[S]

Received for publication, March 2, 2012, and in revised form, March 29, 2012 Published, JBC Papers in Press, April 4, 2012, DOI 10.1074/jbc.M112.358309

Néstor García-Rodríguez[‡1], María del Carmen Díaz de la Loza[‡], Bethany Andreson[§], Fernando Monje-Casas[‡], Rodney Rothstein[¶], and Ralf Erik Wellinger[‡2]

From the [‡]Centro Andaluz de Biología Molecular y Medicina Regenerativa (CABIMER), Universidad de Sevilla-CSIC, 41092, Sevilla, Spain, the [§]Department of Biological Science, Columbia University, New York, New York 10027, and the [¶]Department of Genetics & Development, Columbia University Medical Center, New York, New York 10032

Background: The P-type ATPase Pmr1 provides a major route for cellular detoxification of manganese.
Results: Disregulation of Mn^{2+} homeostasis impairs genome replication and cell cycle progression.
Conclusion: Genome instability and endomitosis can be triggered by alterations in cytosolic or Golgi Mn^{2+} levels.
Significance: The Mn^{2+}-dependent cell cycle defects might explain disease phenotypes observed in Hailey-Hailey patients having mutations in the human *PMR1* orthologue *ATP2C1*.

Manganese is an essential trace element, whose intracellular levels need to be carefully regulated. Mn^{2+} acts as a cofactor for many enzymes and excess of Mn^{2+} is toxic. Alterations in Mn^{2+} homeostasis affect metabolic functions and mutations in the human Mn^{2+}/Ca^{2+} transporter ATP2C1 have been linked to Hailey-Hailey disease. By deletion of the yeast orthologue *PMR1* we have studied the impact of Mn^{2+} on cell cycle progression and show that an excess of cytosolic Mn^{2+} alters S-phase transit, induces transcriptional up-regulation of cell cycle regulators, bypasses the need for S-phase cell cycle checkpoints and predisposes to genomic instability. On the other hand, we find that depletion of the Golgi Mn^{2+} pool requires a functional morphology checkpoint to avoid the formation of polyploid cells.

Correct ion homeostasis is essential for the control of biochemical processes in eukaryotic cells. This is the case of the trace element Mn^{2+} that is required as a cofactor for a wide range of enzymes located in every cellular compartment (1, 2). In addition to serving as an essential enzymatic co-factor, Mn^{2+} can also be toxic and heavy exposure to this ion has been shown to result in a central nervous system disorder resembling parkinsonism, more specifically known as manganism (3, 4).

The *Saccharomyces cerevisiae* gene *PMR1* encodes a Golgi-localized ATPase that transports Ca^{2+} and Mn^{2+} ions from the cytosol into the Golgi lumen (5–7). *PMR1* is evolutionarily conserved from yeast to humans and disruption of one allele of the *PMR1* ortholog ATP2C1 leads to Hailey-Hailey disease in humans (8). Single point mutations that change the ion selectivity of Pmr1 have been described (9, 10), making it possible to distinguish between Ca^{2+}- and Mn^{2+}-specific phenotypes. While Ca^{2+} is required for protein sorting, Mn^{2+} serves as an essential co-factor for *N*- and *O*-linked protein glycosylation in the secretory pathway (5, 11). Other *pmr1*Δ-dependent phenotypes are based on the accumulation of Mn^{2+} in the cytosol that alter reverse transcriptase and telomerase activities (12, 13), activate target of rapamycin (TOR)[3] signaling (14) or permit the scavenging of oxidative radicals (7).

In *S. cerevisiae*, the budding cycle is tightly coupled to the central events of the cell cycle to ensure that genetic information is correctly transferred from mother to daughter. The cyclin-dependent kinase (CDK) Cdc28 is the key component of the mechanism that controls the timing of different cell cycle events. Cdc28 is activated by the alternate association of different cyclins, whose expression is cell cycle regulated, and thereby permits the phosphorylation of different substrates at different times (15). G1-phase cyclins (Cln1–3) are involved in the G1 to S-phase transition promoting bud emergence, spindle pole body duplication and activation of B-type cyclin expression. The early expressed B-type cyclins Clb5 and Clb6 are required for the initiation of DNA replication and progression through S-phase. M-phase cyclins (Clb1–4) are required for spindle formation and the initiation of mitosis. M-phase cyclins also prevent mitotic exit and cytokinesis, and therefore, their activity must be eliminated to allow polarized protein secretion to the bud neck and cell division to take place (16). In addition to being regulated by the association with different cyclins, Cdc28 can also be regulated by post-translational modifications mediated by the morphology checkpoint protein Swe1 (Wee1 in *Schizosaccharomyces pombe*). Swe1 inhibits the kinase activity of Cdc28 complexed with certain B type cyclins including Clb2 and, to a lesser extent, Clb3 and Clb4 by phosphorylation of tyrosine 19 (Y19) causing a delay in G2/M transition (17, 18). The essential coordination between cell cycle progression and

* This work was supported, in whole or in part, by grants from the National Institutes of Health (GM50237) (to R. R.), the Spanish Ministry of Science and Innovation (BIO2006-08051 and BFU2010-21339), and the Junta de Andalucía (P08-CTS-04297) (to R. E. W.).

[S] This article contains supplemental Table S1 and Figs. S1 and S2.

[1] Recipient of a pre-doctoral training grant from the University of Seville/El Monte Foundation.

[2] To whom correspondence should be addressed: Department of Molecular Biology, Centro Andaluz de Biología Molecular y Medicina Regenerativa (CABIMER), Universidad de Sevilla-CSIC, Av Américo Vespucio s/n, 41092, Sevilla, Spain. Tel.: 0034-954467789; Fax: 0034-954461664; E-mail: ralf.wellinger@cabimer.es.

[3] The abbreviations used are: TOR, target of rapamycin; CDK, cyclin-dependent kinase; HU, hydroxyurea; RIs, replication intermediates; RF, replication fork; LOH, loss of heterozygosity.

the budding cycle is ultimately maintained by the presence of a checkpoint that blocks Swe1 degradation, thus delaying mitosis in response to defects in growth or bud formation. This checkpoint appears to be triggered by abnormalities in the actin cytoskeleton (19, 20) as well as cell size (21).

Evidence of a link between Mn^{2+}, DNA replication, and cell cycle progression came from different observations. Mutants coding for temperature-sensitive (*ts*) alleles of the Mn^{2+}-dependent, putative ER-localized lipid phosphatase Cdc1, exhibit a small-bud growth arrest that is identical to the phenotype displayed by Mn^{2+}-depleted cells (22–24). On the other hand, *PMR1* mutants are sensitive to the replication inhibitor hydroxyurea (HU) (25) and exhibit negative genetic interactions with mutants impaired in replication initiation and progression (26, 27). We explored the molecular impact of altered Mn^{2+} homeostasis and dissected the influence of cytoplasm Mn^{2+} overload *versus* depletion of Golgi-hosted Mn^{2+}. Our results indicate that excess of cytosolic Mn^{2+} challenges the replication machinery and is responsible for impaired DNA synthesis, transcriptional up-regulation of G1/S cyclins, bypass of Rad53/Mec1 checkpoint functions and increased DNA damage. In contrast, Golgi-linked cell polarity defects appear to activate the Swe1-dependent morphology checkpoint to prevent polyploidy. Our results clearly demonstrate that Pmr1 is needed to buffer alterations in Mn^{2+} levels, which would otherwise cause loss of cell cycle control, genetic instability, and multinucleation, primary events in tumor formation in higher eukaryotic cells.

EXPERIMENTAL PROCEDURES

Yeast Strain, Plasmids, and Growth Conditions—Yeast strains used in this study are listed in supplemental Table S1. Gene deletions were constructed by PCR-based methods using pFA6a-kanMX6 (28), pAG32 (EUROSCARF), and pFA6a-klLEU2MX6 (kindly provided by B. Pardo) as template plasmids. Regulated P_{GAL} expression of Pmr1 was constructed by PCR-based methods using template plasmid pFA6a-kanMX6-PGAL1 (28). Point mutants *pmr1-Q783A* and *pmr1-D53A* were constructed using an *in vivo* site-directed mutagenesis as described previously (29). *VCX1-M1* was expressed from high-copy yeast-expression plasmid p2UGpd (gift of K. Hirschi), containing the strong constitutive *GPD* promoter. *ATX2* was cloned into the BamHI and SacI sites of p2UGpd. Standard yeast growth conditions and genetic manipulations were used. All experiments were carried out in the corresponding Synthethic Complete (SC) medium, except for microarray experiments and the drop test shown in supplemental Fig. S1*C* (*left*) that were carried out in YPAD medium.

Cell Cycle Analysis—Samples for flow cytometry were prepared following standard procedures and analyzed on a FACScalibur (Becton Dickinson). For G1 synchronization, cells were incubated for 1 h in 1 μg/ml α-factor (RP-4582, Biomedical S.L.) and supplemented with the same amount of fresh α-factor for another hour. Cells were released from α-factor treatment by washing three times in pre-warmed, fresh media.

Analysis of Replication Intermediates—Cells were arrested with sodium azide (0.1% final concentration) and cooled down on ice. Total DNA was isolated, digested with restriction enzymes, and resolved by two-dimensional gel electrophoresis as described previously (30), then transferred onto a Hybond-XL membrane and subsequently hybridized with specific ^{32}P-labeled probes. Signals were quantified using a PhosphorImager Fujifilm FLA-5100 and the ImageGauge program. The relative intensity of replication intermediates was normalized to the signal intensity obtained in the 1n-spot (non-saturating exposure).

Western Blotting and in Situ Kinase Assay—Yeast protein extracts were prepared from $\sim 10^8$ cells by trichloroacetic acid precipitation as described (31). Protein extracts for immunoblotting were separated by sodium dodecyl sulfate-polyacrylamide gel electrophoresis (SDS-PAGE), using 8% polyacrylamide (37.5:1) and 15% polyacrylmide (77:1) gels for Rad53 and Sml1, respectively. Antibodies used for Western blot include anti-Rad53 (yC-19) antibody (SC-6749, Santa Cruz Biotechnology), anti-Adh1 antibody (AB1202, Chemicon International), anti-Sml1 antibody (R. Rothstein) and anti-Hxk1 antibody (H. Riezman, University of Geneve, Switzerland). Protein extracts for Rad53 *in situ* kinase assay were run on a SDS-8% polyacrylamide (37.5:1) gel, and the autophosphorylation reaction was performed as described (32).

Microarray Analysis—Gene expression profiles were determined by using the 3′-expression microarray technology by Affymetrix platform at the Genomics Unit of CABIMER (Seville, Spain). Total RNA from yeast cells grown on YPD at 30 °C to mid-log-phase was isolated using the RNeasy® Midi kit (Qiagen). Synthesis, labeling, and hybridization of cRNA to GeneChip® Yeast Genome 2.0 Arrays was performed with RNA from 3 independent cultures of each strain. The resulting data were reprocessed using the Robust Multi-array Average (RMA) method. The following statistical data analyses were performed using the limma package (*affylmGUI* interface) of the *R* Bioconductor Project. More than 1.8-fold changes with 95% confidence levels (FDR-adjusted p values<0.05) were considered to be significant. The microarray data from this publication have been submitted to the GEO database and assigned the identifier GSE29420.

A-Like Faker (ALF) Assay—The formation of a-mating cells from MATα strains was scored as described (33) with some modifications. Briefly, MATα strains were grown on YPAD plates for 3 days to obtain single colonies. Each ALF frequency value was obtained by the average of at least two fluctuation tests of four independent colonies each. A-like faker cells were selected by growing on YPAD plates overnight at 30 °C. Cells were transferred onto a mating tester lawn of MATα by replica plating followed by incubation at 30° overnight. The mated lawn was then replica plated to Synthetic Dextrose (SD) medium, and colonies were counted. Total cells were grown on YPAD plates.

Microscopy—Rad52-YFP foci levels were analyzed in mid-log-phase cells bearing plasmid pWJ1213 (R. Rothstein). Approximately 300 cells derived from three independent transformation experiments were analyzed for each strain. Meta- and anaphase entry were assessed by spindle (tubulin staining) and nuclear morphology (DAPI) as described (34). For visualization of chromosome IV tagged with GFP, cells were grown at an $A_{600} = 0.2$ and fixed as described (35). Approximately 200 cells from at least three independent experiments were analyzed for each strain. Microscope images were obtained at 25 °C

by projection of a series of focal plane images derived from wide-field fluorescence microscopy (DM-6000B, Leica) at 100× magnification using A4 and L5 filters and a digital charge-coupled device camera (DFC350, Leica). Pictures were processed with LAS AF (Leica). For bud emergence analysis, cells were synchronized with α-factor and released in fresh medium for 90 min. Samples were taken every 15 min, fixed (3,7% formaldehyde), and observed under a light microscope. For each time point, 200 cells were counted and the fraction of cells with no bud, a small bud (smaller than one half of the yeast cell) or a large bud (equal or larger than one half of the yeast cell) was documented. Chitin deposition was visualized using calcofluor white (F3543, Sigma) as described previously (36). Filamentous actin was visualized using rhodamine-phalloidin (P2141, Sigma) as described (37). For septin ring visualization, cells were transformed with the plasmid pLP17 (38) expressing Cdc12 tagged with GFP. At least 200 cells derived from two independent transformation experiments were analyzed for each strain.

RESULTS

Excess of Cytosolic Mn^{2+} Impairs DNA Synthesis and S-phase Progression—Pmr1 is a key regulator of the intracellular Mn^{2+} levels, thus offering the possibility to investigate the impact of impaired Mn^{2+} homeostasis on cell cycle progression. First, we determined the fate of S-phase progression by FACS analysis in *pmr1*Δ. Prior to S-phase release, cells were synchronized in G1/S phase with α-factor and HU. Note that HU provides complete activation of early replication origins but limits fork progression (39). Interestingly, *pmr1*Δ cells were slightly delayed in S-phase progression and remained in G2/M-phase longer than wild type (WT) cells (Fig. 1, *A*, $-MnCl_2$). Addition of extracellular $MnCl_2$ (Fig. 1, *A*, $+MnCl_2$) exacerbated this delay in *pmr1*Δ cells (S-phase peaked after 80 min) but did not affect WT cells (S-phase peaked after 40 min), whereas the addition of extracellular $CaCl_2$ did not affect S-phase progression (supplemental Fig. S1*A*) indicating a Mn^{2+}-dependent delay. To further confirm the specific role of Mn^{2+} in S-phase defects we generated two previously described separation-of-function mutants, *pmr1-Q783A* and *pmr1-D53A*, which transport almost exclusively either Ca^{2+} or Mn^{2+}, respectively (9, 10). Only Mn^{2+}-transport-deficient mutant (*pmr1-Q783A*) showed a delay in S-phase progression in the presence of $MnCl_2$ (supplemental Fig. S1*B*). It is important to note that *pmr1-Q783A* is not a full loss-of-function mutant since it is not as sensitive to $MnCl_2$ as the *pmr1*Δ mutant (supplemental Fig. S1*C*). To rule out that impaired Mn^{2+} supply of the secretory pathway is the cause of S-phase defects, we transformed *pmr1*Δ cells with a plasmid containing a mutant allele of the vacuolar membrane Ca^{2+}/H^+ exchanger *VCX1* (*VCX1-M1*). Vcx1-M1 has enhanced Mn^{2+}/H^+ exchange and was previously found to suppress the Mn^{2+} toxicity phenotype of *pmr1*Δ (40)(supplemental Fig. S1*D*) and, indeed, high-dosage expression of *VCX1-M1* in *pmr1*Δ partially suppressed S-phase transition defects caused by $MnCl_2$ addition (Fig. 1*B*). Finally, by overexpression of the Golgi membrane protein coding *ATX2* gene, we further proved that an increase in cytosolic Mn^{2+} would lead to an S-phase delay (Fig. 1*C*). Atx2 works in opposite directions to Pmr1 to control manganese homeostasis and *ATX2* overexpression has been shown to resemble the Mn^{2+} sensitivity phenotype of *pmr1*Δ (41) (supplemental Fig. S1*E*). Importantly, in the presence of 3 mM $MnCl_2$, *ATX2* overexpression in WT cells reconstituted the same S-phase delay pattern as observed in *pmr1*Δ cells. In previous studies, cytosolic Mn^{2+} levels were determined to be 5–20-fold higher in *pmr1* mutants (7, 42), and therefore we assessed whether the extracellular addition of high $MnCl_2$ concentrations to WT cells would mimic the S-phase transition delay observed in *pmr1*Δ mutants (supplemental Fig. S1*F*). Addition of 10 mM $MnCl_2$ caused a profound delay in S-phase transit and a further increase to 25 mM $MnCl_2$ even prevented WT cells to enter into S-phase. Taken together, these results strongly suggest that cytosolic Mn^{2+} overload delays S-phase transit.

To test whether the delayed S-phase transit in *pmr1*Δ mutants was due to impaired origin firing and/or slow DNA synthesis, we analyzed the fate of *r*eplication *i*ntermediates (RIs) at the molecular level by two-dimensional gel analysis (Fig. 1*D*). To do so, we compared the molecular pattern and appearance of RIs from origin ARS305 (probe A) and progressing along chromosome III (close to ARS305, probe B; further downstream of ARS305, probe C) (43). Upon release from HU arrest, within 20 min the amount of RIs at and close to ARS305 dropped 2–3-fold in the WT and replication was completed within 60 min (Fig. 1*D*, *probes A* and *B*). However, consistent with slower replication in *pmr1*Δ cells, the amount of RIs remained constant within 40 min and replication was completed within 80 min. No obvious differences were visible comparing the two-dimensional pattern of RIs (bubble and simple-Y shaped structures) nor did we detect the appearance of unusual RIs structures in *pmr1*Δ cells. From these results we conclude that the increase in intracellular Mn^{2+} contributes to slower replication fork (RF) progression in *pmr1*Δ cells. In addition to defects in fork progression, we noticed that the relative amount of RIs at the onset of replication appeared to be lower in *pmr1*Δ cells (see Fig. 1*D*, *probe A*). This finding prompted us to analyze the timing of replication initiation in *pmr1*Δ cells (supplemental Fig. S1*G*). Upon α-factor release into low levels of HU to limit fork progression, samples were taken every 4 min and subjected to two-dimensional gel analysis. While in WT cells the first RIs in ARS305 were present within 8 min, in *pmr1*Δ cells RIs were visible about 12 min after S-phase entry. Thus, replication initiation and fork progression are affected in *pmr1*Δ cells.

Late Origin Activation Is Required to Prevent Genome Instability under Condition of Increased Cytosolic Mn^{2+}—To determine if the fork progression delay has an impact on the onset of late origin firing activation, we compared the replication timing between the early firing origin ARS607 and the late firing origin ARS603 (Fig. 2*A*), both located in chromosome VI. As for ARS305, ARS607 showed a defect in replication initiation, as seen by the lower amount of RIs after HU release, and a slowdown of RF progression in *pmr1*Δ cells suggesting that this is a general feature. Interestingly RF progression and the temporal activation of late origin ARS603 firing were delayed by 20 min in *pmr1*Δ mutants. Importantly, *pmr1*Δ cells are capable of initiating origin-firing at ARS603, indicating that the *pmr1*Δ-de-

pendent S-phase delay is not mediated by the inhibition of late origin activation.

CLB5 encodes a B-type cyclin that activates Cdc28p to promote initiation of DNA synthesis and *clb5*Δ cells have been shown to present a prolonged S-phase as a result of failure to activate late origins (44, 45). We reasoned that if *pmr1*Δ cells were not affected in late origin activation, *pmr1*Δ *clb5*Δ mutant might show a synergistic effect in

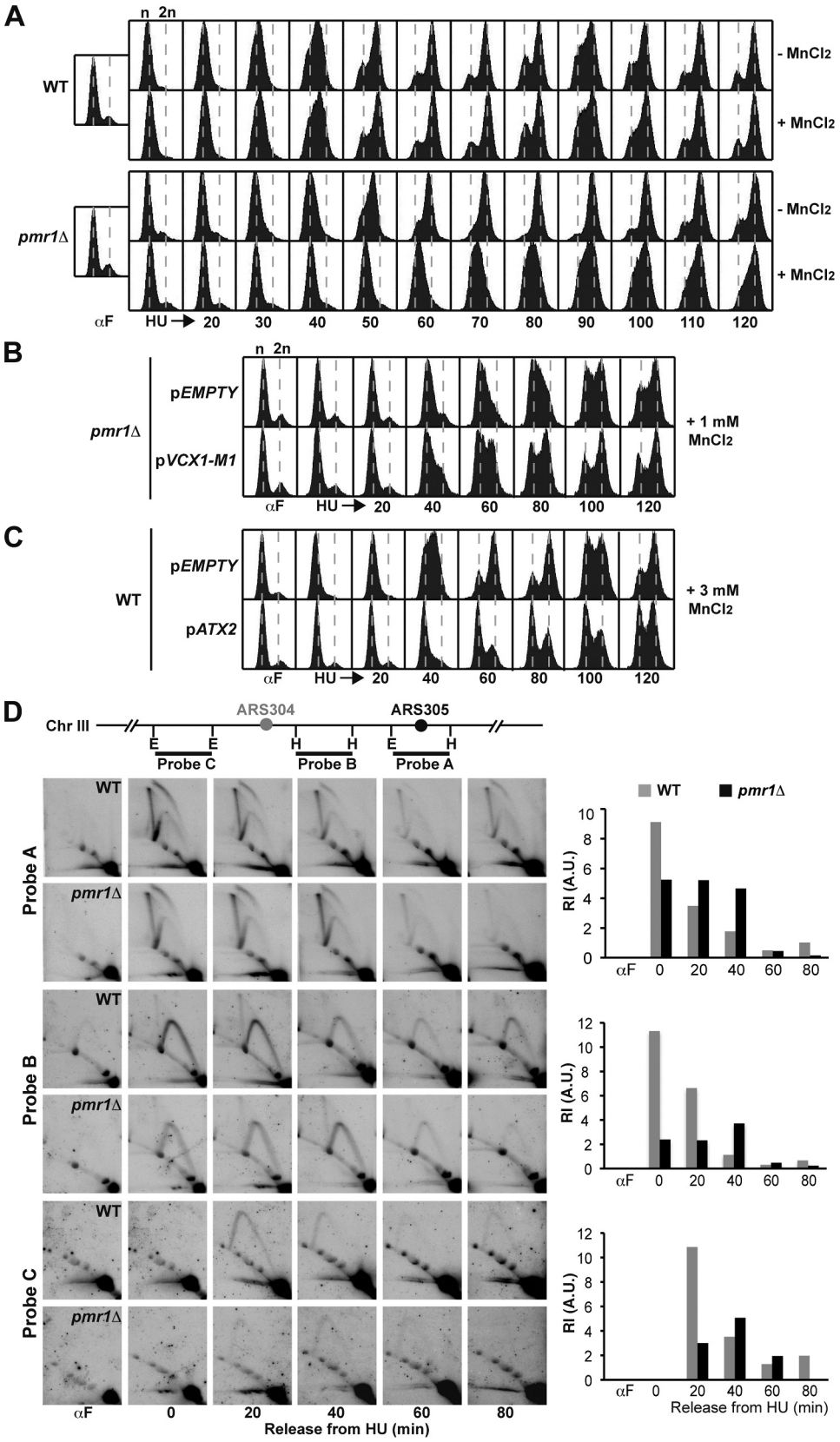

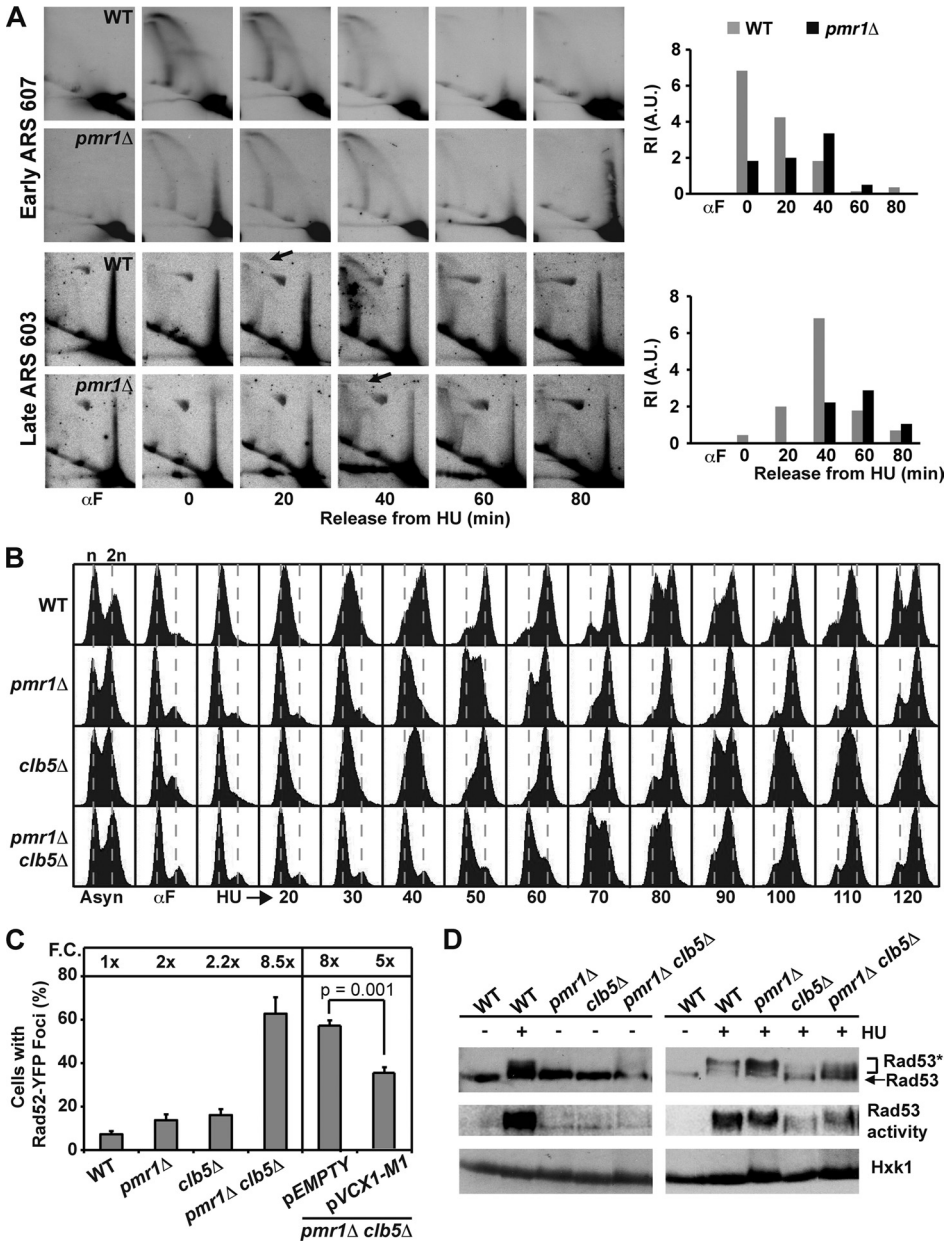

FIGURE 2. **Clb5 is needed to prevent genomic instability under conditions of cytosolic Mn $^{2+}$ overload.** *A*, two-dimensional gel analysis of early ARS607 and late ARS603 ori-firing. *Arrows* indicate bubble-shaped RIs. DNA samples were digested with PstI or BamHI to analyze ARS607 or ARS603 respectively. *B*, FACS analysis of S-phase progression in WT (BY4741), *clb5*Δ (NGY101), *pmr1*Δ (NGY051), and *pmr1*Δ *clb5*Δ (NGY103) synchronized at G1/S with α-factor and HU (200 mM) prior to S-phase release. *C*, DNA repair centers were determined by Rad52-YFP foci formation in strains described in Fig. 2*B* (*left*), in *pmr1*Δ *clb5*Δ harboring a plasmid containing a mutant allele of *VCX1* (p*VCX1-M1*), and the empty vector (p2UGpd) (*right*). Error bars represent S.D. of three independent experiments. Fold changes (*F.C.*) compared with the WT are indicated (n>300). *D*, Western blot analysis of Rad53 protein and *in situ* autophosphorylation assay for Rad53 activity without treatment (*left*) or after 3 h in the presence of 200 mM HU (*right*) in strains described in Fig. 2*B*. The phosphorylated form of Rad53 is indicated (*). Hxk1 protein was used as a loading control.

S-phase progression. For this purpose, we generated *pmr1*Δ *clb5*Δ double mutants and followed cell cycle progression by FACS analysis (Fig. 2*B*). As expected, while *pmr1*Δ and *clb5*Δ single mutants were slightly delayed in S-phase progression, the double mutant showed an additive delay (S-phase peaked after 80 min).

FIGURE 1. **Excess of cytosolic Mn^{2+} impairs S-phase progression.** *A*, FACS analysis of S-phase progression in WT (BY4741) and *pmr1*Δ cells (NGY051) synchronized in G1/S with α-factor (αF) and HU (200 mM) prior to release into fresh medium. Note that HU permits ori-firing but restricts replication elongation. $MnCl_2$ (1 mM) was added after release from αF where indicated. Samples were taken at the indicated times (min). *B*, FACS analysis of *pmr1*Δ cells (NGY051) transformed with a plasmid coding for a mutant allele of the vacoluar Ca^{2+} transporter *VCX1* that instead transports Mn^{2+} into the vacuole (p*VCX1-M1*). An empty vector (p2UGpd) was used as control. $MnCl_2$ (1 mM) was added after release from αF into fresh medium. *C*, FACS analysis of WT cells (BY4741) transformed with an *ATX2* overexpressing plasmid leading to a cytosolic Mn^{2+} increase. An empty vector (p2UGpd) was used as control. $MnCl_2$ (3 mM) was added after release from αF. *D*, two-dimensional gel analysis of RF progression along chromosome III in WT (BY4741) and *pmr1*Δ (NGY051) cells. Cells were synchronized at G1/S with αF and HU (200 mM) prior to S-phase release. DNA samples were digested with EcoRV (*E*) and HindIII (*H*) as indicated (*top*). Replication is initiated at ARS305 (bubble-shaped molecules; *probe A*) and passive fork progression is detected toward the left arm of chromosome III (simple-Y shaped molecules; *probes B* and *C*). Note that origin ARS304 (*gray*) remains dormant. Quantification of total RIs is shown to the *right*.

Next, we asked if replication forks might be more prone to DNA damage due to delayed replication fork progression. To assess this possibility, we measured replicative damage by monitoring the formation of DNA repair centers that are dependent on the homologous recombination protein Rad52 (46) (Fig. 2*C*, *left*). An increase of Rad52-YFP foci was evident in *pmr1*Δ and *clb5*Δ simple mutants. However, in the double mutant, the formation of DNA repair centers was boosted with more than 60% of the cells containing Rad52-YFP foci. To assess whether DNA damage in *pmr1*Δ *clb5*Δ mutants is mediated by cytosolic Mn^{2+} overload, this mutant was transformed with plasmid p*VCX1-M1* to decrease the cytosolic Mn^{2+} levels. Interestingly, we observed a statistically significant reduction in the formation of Rad52-YFP foci in cells overexpressing *VCX1-M1* (Fig. 2*C*, *right*), indicating that cytosolic Mn^{2+} overload is indeed promoting genetic instability. To preserve RF integrity, intra-S checkpoint activation leads to the phosphorylation of the checkpoint sensor Rad53 (43). Interestingly, we found that Rad53 phosphorylation was reduced in HU-treated *clb5*Δ mutants, possibly due to reduced number of replicons per cell (Fig. 2*D*). Thus, the combination of having less replicons and slow replication forks might account for the extreme delay in S-phase progression and the massive formation of DNA repair centers in *pmr1*Δ *clb5*Δ mutants.

Deletion of PMR1 Leads to Transcriptional Up-regulation of Factors Involved in Cell Cycle and Polarity—Eukaryotic cell cycle is carefully regulated to ensure that genetic material is duplicated precisely before cell division takes place. In *S. cerevisiae*, a single Cdk, Cdc28 associates with multiple cyclins to regulate the cell cycle. To investigate whether defects in S-phase progression might lead to an alteration in the cellular gene expression profile in an attempt to readjust the cell cycle, we analyzed total mRNA levels in *pmr1*Δ mutants by microarray analysis (Fig. 3*A*, accession number GSE29420 at GEO database). In *pmr1*Δ cells, a significant number of genes involved in sugar (22 of 241) and iron metabolism (5 of 241) were down-regulated, while genes associated with the cell cycle and stress response (30 of 129), cell polarity (18 of 129), and the regulation of kinase activity (13 of 129) were up-regulated. Importantly the transcriptional up-regulation of Cdc28 as well as of cyclins involved in the G1/S transition of the cell cycle such as *CLB5/6*, *CLN1/2*, and *PCL1/2* appear to be relevant, because this finding is in concordance with the previously reported loss of viability of *pmr1*Δ *cln1*Δ *cln2*Δ triple mutant (47). Remarkably, one of the up-regulated genes was *SRL3* (suppressor of rad53 Lethality) (48), a potential substrate of the Cdc28 kinase. To verify *SRL3* up-regulation, we tested by tetrad analysis (Fig. 3*B*) if the *PMR1* deletion could suppress *rad53*Δ and *mec1*Δ lethality, mutants known to be suppressed by *SRL3* overexpression (48). As this appeared to be true, we further characterized the lack of Rad53-dependent Sml1 protein degradation in response to MMS-induced DNA damage by Western blot analysis of *pmr1*Δ *rad53*Δ mutants (Fig. 3*C*). An assay based on counter-selection of a plasmid harboring *RAD53* revealed that only cells lacking the Mn^{2+}-(*pmr1-Q783A*) but not Ca^{2+}-pump function (*pmr1-D53A*) suppressed *rad53*Δ lethality (Fig. 3*D*). In agreement with this observation, lowering cytosolic Mn^{2+} by transport to the vacuolar space by *Vcx1-M1* restored lethality of *pmr1*Δ *rad53*Δ cells (Fig. 3*E*). Finally, we determined that *pmr1*Δ *rad53*Δ *srl3*Δ triple mutants were unviable.[4] It is thus conceivable that the bypass of G1/S checkpoint functions occurs in response to G1/S phase transition constraints mediated by cytosolic Mn^{2+} overload.

Golgi Mn^{2+} Pool Depletion Activates the G2/M Morphology Checkpoint to Avoid Polyploidy—As previously mentioned, FACS analysis of S-phase progression in *pmr1*Δ cells revealed a substantial delay in G2/M phase entry or exit (see Fig. 1*A*). We suspected that this delay might be related to the observed transcriptional up-regulation of Swe1 (see Fig. 3*A*), a protein kinase involved in regulating G2/M transition (17). To test if this was the case, we generated *pmr1*Δ *swe1*Δ double mutants and followed cell cycle progression by FACS analysis (Fig. 4*A*). Interestingly, the absence of Swe1 liberated *pmr1*Δ cells from the G2/M delay (see Fig. 4*A*, after 120 min). To further confirm this observation, we placed the expression of *PMR1* under the control of the repressible *GAL1* promoter and followed progression though meta- and anaphase (Fig. 4*B*). Upon repression of *PMR1* transcription, we observed a delay in meta- and anaphase progression (Fig. 4*B*, *red circles*), which did not occur in a *swe1*Δ background (Fig. 4*B*, *blue triangles*) confirming that Swe1 mediates the G2/M delay.

The bypass of the G2/M delay in *pmr1*Δ might lead to uncontrolled chromosome segregation resulting in loss of heterozygosity (LOH). To assess this possibility, we measured LOH frequency by the formation of a-like faker cells (33) (ALF, Fig. 4*C*). Unexpectedly, while *pmr1*Δ and *swe1*Δ single mutants did not show a statistically significant change relative to the WT, LOH was suppressed in *pmr1*Δ *swe1*Δ mutants. Previous studies have concluded that Swe1 does not play a role during the cell cycle in normal, unperturbed conditions (17). In contrast, Swe1 is part of the morphogenesis checkpoint and, in response to perturbations that prevent bud formation, inhibits mitotic progression through negative regulation of Clb/Cdk (49). Overexpression of the mitotic cyclin Clb2 has been shown to result in the accumulation of multinucleated cells in *swe1*Δ background (50). Multinucleation has also been observed in *pmr1*Δ as well as *swe1*Δ during meiosis (51, 52). Therefore, the presence of more than one copy of chromosome III (chr. III) could account for LOH suppression. We examined the nuclear morphology of *pmr1*Δ *swe1*Δ mutants (Fig. 5*A*). Microscopical analysis revealed that about 41% of the cells contained multiple nuclei (DAPI staining) and multiple copies of chr. IV (GFP-tagged) and that the cellular diameter exceeded 8 μm in at least 35% of the total cell population. Importantly, we noticed the formation of giant cells, which were prone to undergo spontaneous lysis. A very gentle handling allowed us to confirm the presence of multinucleated cells by FACS (Fig. 5*A*, *right*). Multinucleated cells were evident in *pmr1-Q783A* but not *pmr1-D53A swe1*Δ mutants (supplemental Fig. S2), suggesting that multinucleation was mediated by an Mn^{2+} but not Ca^{2+} transport defect. Moreover, lowering cytosolic Mn^{2+} levels by transport into the vacuole using the mutant allele *VCX1-M1* did not restore normal cell size nor suppress multinucleation, instead these phe-

[4] R. E. Wellinger, unpublished observations.

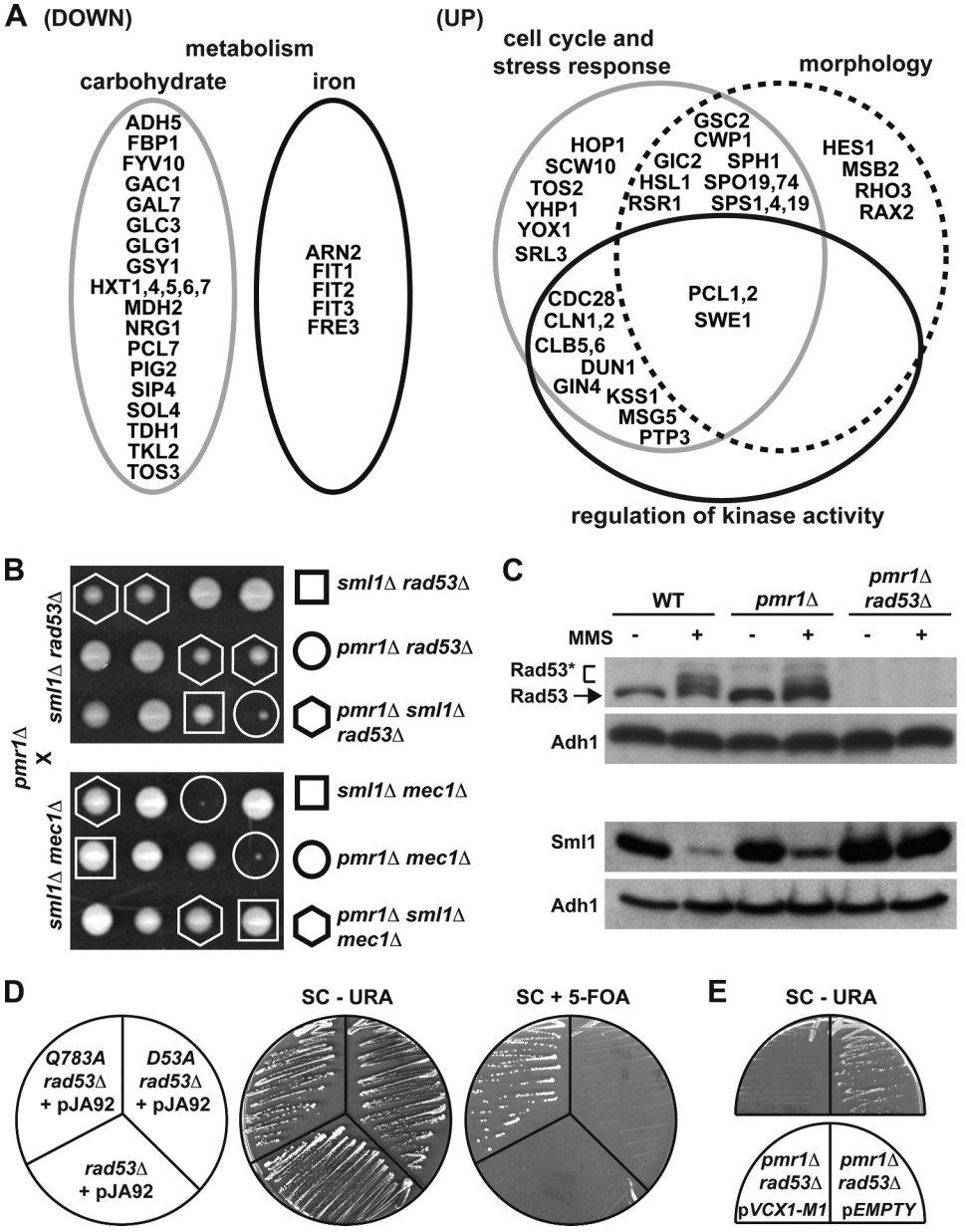

FIGURE 3. **pmr1Δ shows transcriptional up-regulation of factors involved in cell cycle and polarity and bypasses *rad53Δ* and *mec1Δ* lethality.** *A*, microarray analysis of mRNA levels in *pmr1*Δ mutants (NGY035) compared with the WT mRNA levels (BY4742) from cells grown in YPAD medium. Genes whose expression was more than 1.8-fold down or up-regulated and that were significantly enriched for a GO-term are indicated (p value$<$0.002). *B*, tetrad analysis crossing *pmr1*Δ (NGY003) with *rad53*Δ *sml1*Δ (W2105–17B) and *mec1*Δ *sml1*Δ (U963–61A). The genotype of the relevant spores is indicated. *C*, Western blot analysis of Rad53 and Sml1 proteins upon MMS treatment (0.03%) in WT (W303–1A), *pmr1*Δ (NGY003), and *pmr1*Δ *rad53*Δ (W1887–5C). The phosphorylated form of Rad53 is indicated (*). Adh1 protein was used as a loading control. *D*, deficient Golgi Mn^{2+} pump function suppresses the lethality associated with *rad53* deletion. *pmr1-Q783A rad53*Δ (NGY180), *pmr1-D53A rad53*Δ (NGY181), and *rad53*Δ (NGY182) mutants containing plasmid pJA92 (kindly provided by S. Elledge) expressing *RAD53* under its own promoter were streaked onto SC-ura and SC supplemented with 500 mg/ml of 5-fluorotic acid (5-*FOA*). Plasmid loss was deduced by the formation of 5-FOA-resistant cells. *E*, lowering cytosolic Mn^{2+} by transport to the vacuolar space confers lethality to *pmr1*Δ *rad53*Δ cells. Shown is the growth of *pmr1*Δ *rad53*Δ (W1887–5C) transformed with a control vector (p2UGpd) or a plasmid containing a mutant allele of *VCX1* (p*VCX1-M1*) on SC-ura.

notypes appeared to be exaggerated, as seen by a statistically significant increase in cell diameter (Fig. 5*B*). Together these data demonstrate that Golgi Mn^{2+} depletion leads to polyploidy in the absence of an active morphology checkpoint.

Mn^{2+} Depletion Causes Cell Polarity Defects Linked to Protein Glycosylation—Mn^{2+} is needed as a co-factor for the proper action of Golgi hosted mannosyltransferases (53–55) and impaired Golgi Mn^{2+} transport has been shown to cause protein underglycosylation (11). Other studies have shown that mannosyltransferase mutants affected in protein glycosylation display a pronounced delay in bud formation (56, 57). Moreover, *SWE1* mRNA levels are elevated in cells that cannot make a bud (58). To test whether *pmr1*Δ cells were affected in bud formation, we synchronized cells with α-factor at G1-phase prior to release into S-phase, finding that *pmr1*Δ cells showed a delay of 15 min in bud emergence relative to the WT (Fig. 6*A*). We conclude from this experiment that Golgi Mn^{2+} was required for timely bud emergence and that the morphogenesis checkpoint was essential to delay mitosis until a bud was formed.

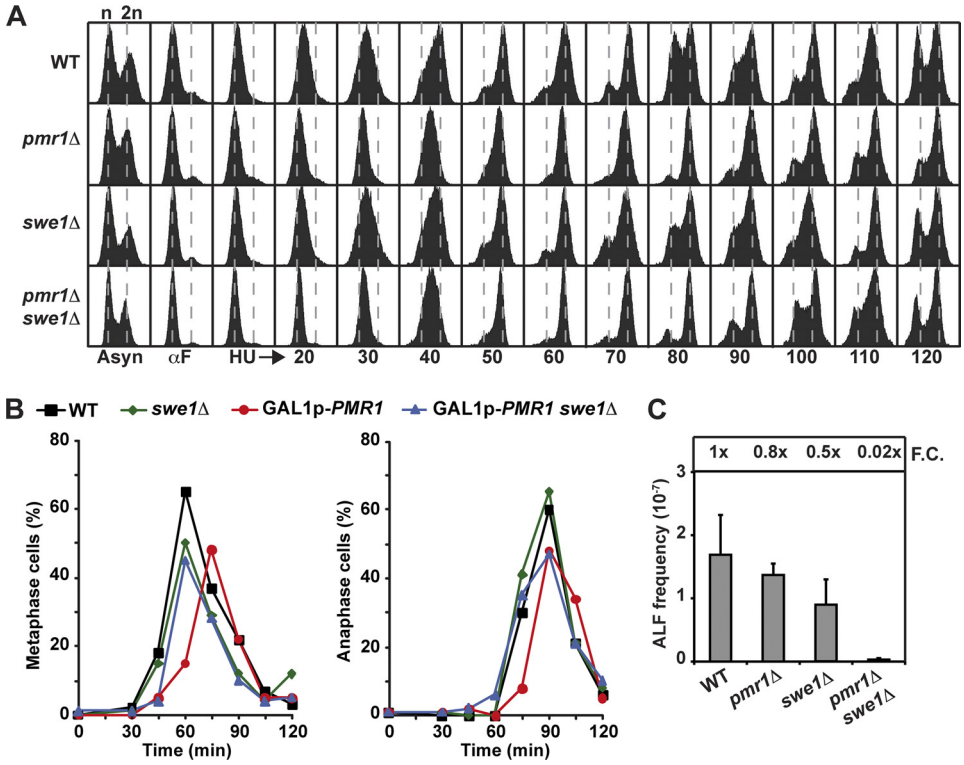

FIGURE 4. **Swe1 prevents premature entry into mitosis.** *A*, FACS analysis of S-phase progression in WT (BY4741), *swe1*Δ (NGY152), *pmr1*Δ (NGY051), and *pmr1*Δ *swe1*Δ (NGY154) synchronized at G1 with α-factor and HU (200 mM) prior to S-phase release. *B*, metaphase 'checkpoint' bypass releases *pmr1*Δ cells from G2/M arrest. For inducible Pmr1 depletion, *PMR1* expression was placed under control of the *GAL1* promoter. WT (NGY124), *swe1*Δ (NGY131), *GAL1p-PMR1* (NGY144), and *GAL1p-PMR1 swe1*Δ (NGY143) cells were synchronized in G1/S phase with α-factor in the presence of glucose, and cell cycle progression was determined by spindle (tubulin staining) and nuclear morphology (DAPI). Percentages of metaphase and anaphase cells are shown for each time point (n>200). *C*, LOH measured by the formation of a-like fakers (ALF) in strains described in Fig. 4*A*. Error bars represent S.D. of at least two experiments. Fold changes respect to the WT are indicated.

The fact that *pmr1*Δ cells were delayed in bud emergence suggested that they might be defective in polarized growth during the cell cycle. This type of phenotype is often associated with alteration in chitin deposition and inability to properly organize the actin cytoskeleton. Accordingly, analysis of chitin deposition in *pmr1*Δ mutant, which is normally found in the neck region of budded cells and in bud scars, revealed that chitin was delocalized and deposited at elevated levels (Fig. 6*B*). In the case of actin, which is normally organized with actin patches found exclusively in the buds and actin cables oriented toward the tips of the buds, *pmr1*Δ showed a slight defect in the organization with some mislocalized patches (Fig. 6*C*). Interestingly, although chitin deposition was normal in *swe1*Δ cells, a massive accumulation of chitin at the bud emergence site was evident in *pmr1*Δ *swe1*Δ mutants. Moreover, the actin cytoskeleton was clearly depolarized in giant *pmr1*Δ *swe1*Δ cells, showing actin patches randomly distributed. Impaired bud neck formation was even more evident looking at septin rings between mother and daughter cells (Fig. 6*D*). Septins were thickened and mislocalized in a substantial fraction of *pmr1*Δ *swe1*Δ cells. These results suggest that Golgi Mn^{2+} is essential to establish or maintain cell polarity, making a functional morphogenesis checkpoint crucial to coordinate budding with G2/M entry in *pmr1*Δ mutants.

DISCUSSION

In this work, we have uncovered a remarkable impact of manganese on DNA synthesis and nuclear segregation (Fig. 7, see figure legend for explanation). Cytosolic Mn^{2+} excess could interfere with the activity of Mg^{2+}-dependent enzymes. It is known that high Mn^{2+} concentration can compromise *e.g.* the *in vitro* activity of the flap endonuclease Rad27 (59) as well as the fidelity of DNA polymerases (60). Mn^{2+} has also been shown to decrease the catalytic activity of reverse transcriptases leading to reduced Ty1 retrotransposition in *pmr1*Δ mutants (12) as well as to alter the fidelity of the telomerase *in vitro* and to induce telomere shortening *in vivo* (13). Moreover, cytosolic Mn^{2+} accumulation in *pmr1*Δ mutants has been shown to increase viral recombinants by affecting RNA-dependent RNA polymerases (61). Although we do not know all enzymatic activities that may be altered in the presence of Mn^{2+}, the impaired function of proteins that take part in DNA synthesis or even DNA polymerases themselves, are likely to contribute to replication slow-down. It is tempting to speculate that cytosolic manganese overload might slow-down the nucleotide incorporation during DNA synthesis causing a reduction in the consumption of dNTPs. *MEC1* and *RAD53* play the essential role of maintaining an adequate nucleotide supply during G1/S transition (48) and a reduced need for dNTPs during DNA synthesis could explain the *pmr1*Δ-dependent suppression of *rad53*Δ and *mec1*Δ lethality. Despite this possibility, suppression of *rad53*Δ lethality was linked to the up-regulation of *SRL3*. Little is known about the function of Srl3, but apparently trancriptional up-regulation of *SRL3* takes part in the activation of the cell wall integrity (CWI) pathway (62). Cytosolic Mn^{2+}

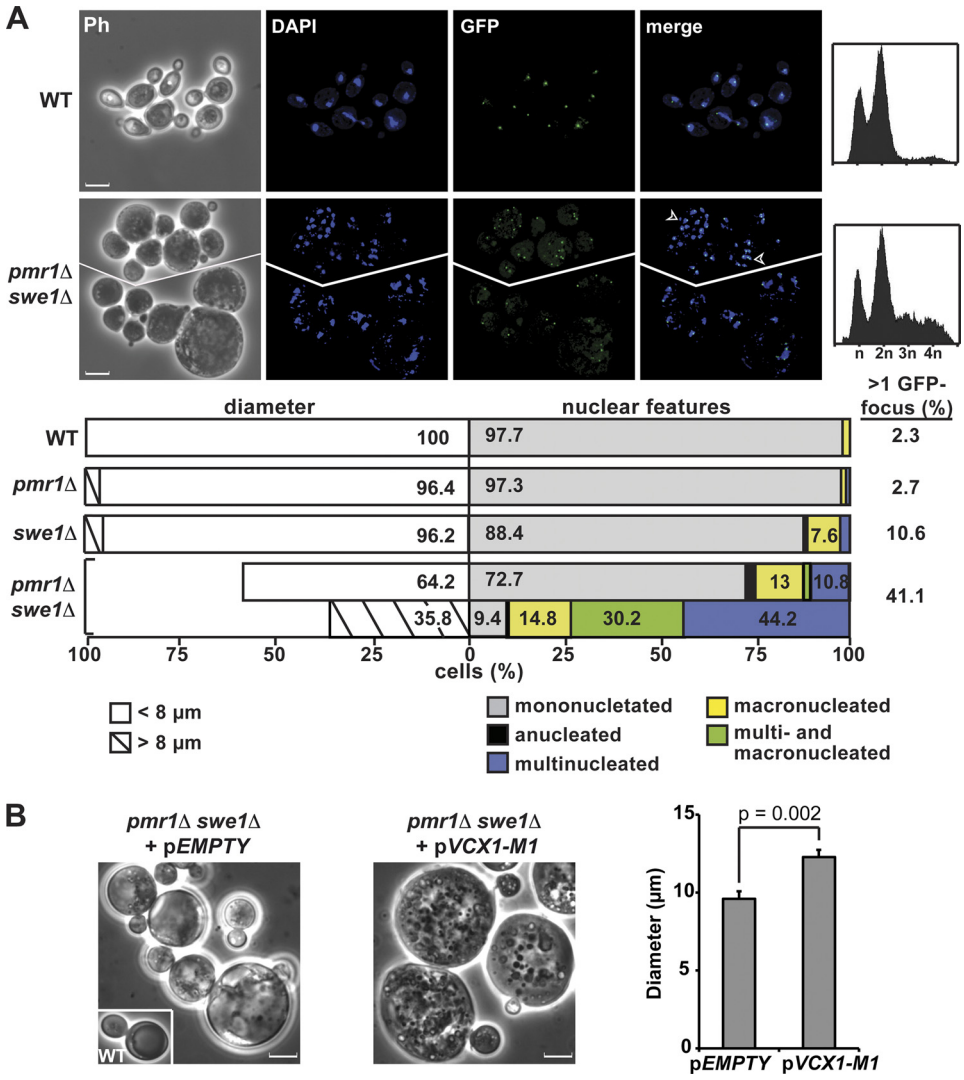

FIGURE 5. **G2/M morphology checkpoint activation avoids polyploidy related to Golgi Mn^{2+} depletion.** *A*, microscopy images of cells (*top left*) and FACS profiles of asynchronous cells (*top right*) are shown. Total genomic DNA was visualized by DAPI staining, while chromosome IV was marked by GFP-binding. *Arrows* indicate multinucleated cells. Bar, 5 μm. Changes in cell diameter and nuclear features of WT (NGY124), *pmr1*Δ (NGY134), *swe1*Δ (NGY131), and *pmr1*Δ *swe1*Δ (NGY126), are indicated below (n>200). *B*, lowering cytosolic Mn^{2+} exacerbates giantism. *pmr1*Δ *swe1*Δ (NGY126) was transformed with a control vector (p2UGpd) or a plasmid containing a mutant allele of *VCX1* (p*VCX1-M1*) and grown on selective media. Microscopy images (*left*) and measure of cell diameter (*right*) are shown (*n* >200). Error bars represent S.D. of three independent experiments.

overload could resemble osmotic stress conditions by which the stress-activated protein kinase (SAPK) Hog1 is activated leading to replication constrains (63). Notably, we find that some of the known Hog1 targets (*e.g.* Hsl1 and Swe1, (64)) were up-regulated in *pmr1*Δ mutants.

We observe that early and late origin activation is clearly delayed but not impaired in *pmr1*Δ mutants, an observation that is in concordance with the previously reported synthetic sick interaction of *pmr1*Δ with mutants of the ORC complex (27). Moreover, lack of Pmr1 invokes the transcriptional up-regulation of Clb5/6, both cyclins needed for the full activation of early and late origins (44, 45). Interestingly, the additive S-phase delay and increase in DNA damage in *pmr1*Δ *clb5*Δ mutants points to the possibility that replisome composition and integrity is challenged by manganese. This might explain the enhanced sensitivity of *pmr1*Δ mutants to DNA damaging agents such as camptothecin, MMS, and 4-NQO (65).[4] Our two-dimensional gel analysis of RIs did not reveal evidence for increased replication fork break down, nor an increase in Holliday junction formation (see Figs. 1*D*, 2*A*, and supplemental Fig. S1*F*). However, replication fork slow-down in *pmr1*Δ cells could mediate a transient uncoupling of leading and lagging strand synthesis, thus increasing the formation of gapped DNA. Evidence for such a possibility is given by the synthetic growth defect of *pmr1*Δ in combination with a lack of proteins that have a role in gap repair such as Rad18, Rad27, or the members of the Rad52 epistasis group (26), as well as the transcriptional up-regulation of the cell-cycle checkpoint serine-threonine kinase Dun1, a regulator of postreplicative DNA repair (66).

Cell cycle progression and the morphogenesis (budding) cycle are tightly coupled to ensure a successful cell proliferation. Dramatic changes in cell polarity that occur in G1 (polarization at the bud site), G2 (depolarization within the bud), and mitosis (repolarization to the bud neck) are triggered by changes in the kinase activity of Cdc28, the universal regulator of cell cycle progression (67). We present data suggesting that

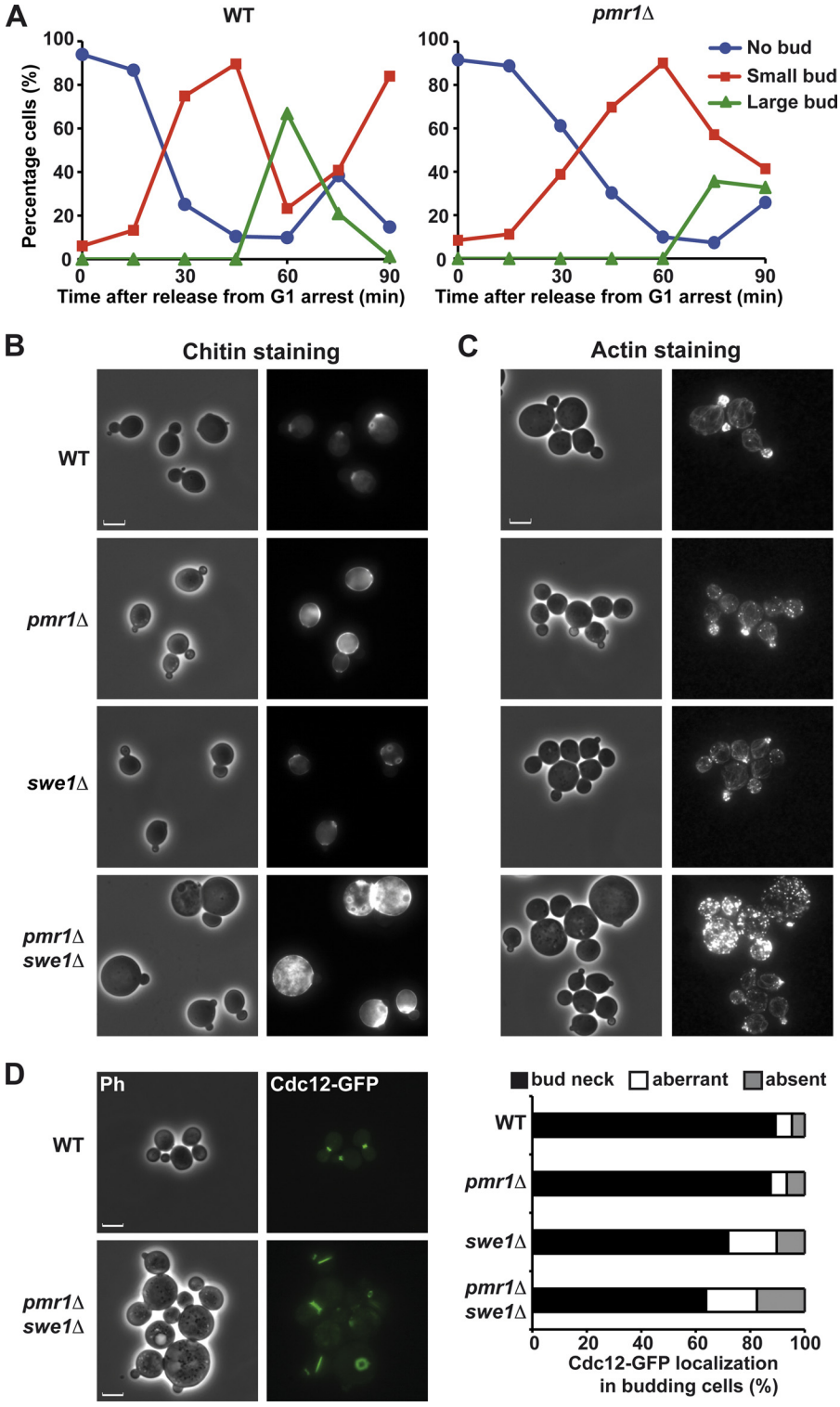

FIGURE 6. **Pmr1 is essential to establish a proper cell polarity.** *A*, WT (NGY124) and *pmr1*Δ (NGY134) cells were synchronized at G1 with α-factor and released in fresh medium for 90 min. For each time point, the fraction of cells with no bud (*blue circle*), small bud (*red square*), and large bud (*green triangle*) was scored (n >200 per point). *B*, chitin and *C*, actin localization in WT (NGY124), *pmr1*Δ (NGY134), *swe1*Δ (NGY131), and *pmr1*Δ *swe1*Δ (NGY126) cells stained with calcofluor white and rhodamine-phalloidin, respectively. *Bar*, 5 μm. Magnification and exposures time were the same for all strains. *D*, WT (W303–1A), *pmr1*Δ (NGY003), *swe1*Δ (NGY120-B), and *pmr1*Δ *swe1*Δ (NGY120-A) cells were transformed with the plasmid pLP17 expressing Cdc12 tagged with GFP and analyzed by fluorescence microscopy. For each strain, the fraction of cells with no septin ring (*gray*), aberrant (*white*), and bud-neck (*black*) localization was documented (n >200). Bar, 5 μm.

the coordination of cell cycle progression and morphogenesis by the morphology checkpoint Swe1 is essential to avoid polyploidy in *PMR1* mutants lacking the Golgi Mn^{2+} pump function. Delayed bud emergence and alterations in chitin deposition indicate that *pmr1*Δ cells are defective in polarized growth. Accordingly, G1-specific cyclin-dependent kinases Cln1/2-

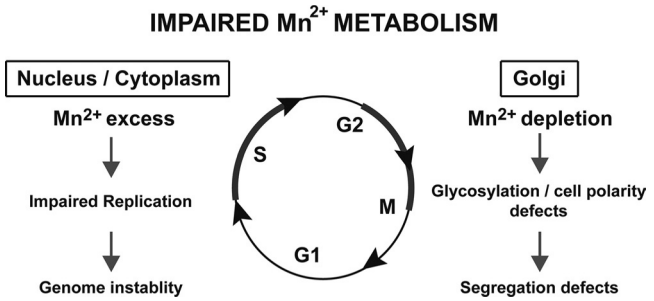

FIGURE 7. **A model for the effect of impaired Mn^{2+} metabolism on cell cycle.** Cytosolic Mn^{2+} overload impairs S-phase progression and leads to genome instability. On the other hand, Golgi Mn^{2+} depletion impairs proper glycosylation of proteins involved in the establishment of cell polarity, leading to segregation defects.

Cdc28 and Pcl1/2-Pho85, which regulate essential events during the G1/S transition and morphogenesis events, such as polarized growth and bud emergence, appear to be up-regulated in cells lacking Pmr1, as a plausible consequence of dealing with difficulties to establish a proper cell polarity. Moreover, cells lacking Pmr1 show genetic interactions with the cell polarity GTPase, Cdc42 (68). Several reports have shown that mannosyltransferase mutants affected in *N*-glycosylation are defective in polarized growth and become dependent on an intact mitotic checkpoint for survival, which provides time to produce a bud (56, 57). Overriding the morphogenesis checkpoint by Clb2 overexpression in these mutants resembles the multinucleation phenotype of *pmr1*Δ *swe1*Δ mutants (56, 57). The fact that some components of the *cis*-Golgi mannosyltransferase complex are Mn^{2+}-dependent enzymes suggests that the function of these enzymes is impaired if the Golgi is not supplied with Mn^{2+} (53–55). Accordingly, *PMR1* mutants are deficient in protein *N*-glycosylation and this phenotype can be partially suppressed by Mn^{2+} addition (11). From these findings, it becomes apparent that Pmr1 acts upstream of *cis*-Golgi mannosyltransferases suggesting that their multinucleation phenotype is epistatic.

The regulation of Mn^{2+} homeostasis has been shown to be highly conserved between yeast and higher eukaryotes (69). Mutations in the human *PMR1* ortholog ATP2C1 cause Hailey-Hailey disease, an autosomal dominant blistering skin disorder (8). Deficient Mn^{2+} homeostasis might be linked to tumor formation in some Hailey-Hailey patients (70) as well as in haploinsufficient ATP2C1$^{-/+}$ mice (71), given the evidence that cytosolic overload and depletion of the Golgi-hosted Mn^{2+} increase the incidence of genetic instability and multinucleation in yeast. Thus, it will be interesting to see whether Mn^{2+}-dependent alterations in replication and checkpoint activities indeed contribute to cancer formation in affected Hailey-Hailey patients.

Acknowledgments—We thank Drs. R. Rao, S. Muend, K. D. Hirschi, S. Elledge, M. A. Resnick, F. Storici, H. Riezman and M. Muñiz for plasmids and reagents; H. Gaillard, J. Manetsberger and B. Pardo for experimental suggestions and critical reading of the manuscript; P. Domínguez, E. García, and M. Pérez from CABIMER Microscopy and Genomic units, for assistance in microscopy and microarray analysis. Control data sets for strain BY4742 have been kindly provided by C. González-Aguilera and A. Aguilera.

REFERENCES

1. Keen, C. L., Ensunsa, J. L., and Clegg, M. S. (2000) Manganese metabolism in animals and humans including the toxicity of manganese. *Met. Ions. Biol. Syst* **37,** 89–121
2. Crowley, J. D., Traynor, D. A., and Weatherburn, D. C. (2000) Enzymes and proteins containing manganese: an overview. *Met. Ions. Biol. Syst* **37,** 209–278
3. Couper, J. (1837) On the effects of black oxide of manganese when inhaled into the lungs. *Br. Ann. Med. Pharmacol.* **1,** 41–42
4. Lucchini, R. G., Martin, C. J., and Doney, B. C. (2009) From manganism to manganese-induced parkinsonism: a conceptual model based on the evolution of exposure. *Neuromol. Med.* **11,** 311–321
5. Rudolph, H. K., Antebi, A., Fink, G. R., Buckley, C. M., Dorman, T. E., LeVitre, J., Davidow, L. S., Mao, J. I., and Moir, D. T. (1989) The yeast secretory pathway is perturbed by mutations in PMR1, a member of a Ca^{2+} ATPase family. *Cell* **58,** 133–145
6. Antebi, A., and Fink, G. R. (1992) The yeast Ca(2+)-ATPase homologue, PMR1, is required for normal Golgi function and localizes in a novel Golgi-like distribution. *Mol. Biol. Cell* **3,** 633–654
7. Lapinskas, P. J., Cunningham, K. W., Liu, X. F., Fink, G. R., and Culotta, V. C. (1995) Mutations in PMR1 suppress oxidative damage in yeast cells lacking superoxide dismutase. *Mol. Cell Biol.* **15,** 1382–1388
8. Hu, Z., Bonifas, J. M., Beech, J., Bench, G., Shigihara, T., Ogawa, H., Ikeda, S., Mauro, T., and Epstein, E. H., Jr. (2000) Mutations in ATP2C1, encoding a calcium pump, cause Hailey-Hailey disease. *Nat. Genet.* **24,** 61–65
9. Wei, Y., Marchi, V., Wang, R., and Rao, R. (1999) An N-terminal EF hand-like motif modulates ion transport by Pmr1, the yeast Golgi Ca(2+)/Mn(2+)-ATPase. *Biochemistry* **38,** 14534–14541
10. Mandal, D., Woolf, T. B., and Rao, R. (2000) Manganese selectivity of pmr1, the yeast secretory pathway ion pump, is defined by residue gln783 in transmembrane segment 6. Residue Asp778 is essential for cation transport. *J. Biol. Chem.* **275,** 23933–23938
11. Dürr, G., Strayle, J., Plemper, R., Elbs, S., Klee, S. K., Catty, P., Wolf, D. H., and Rudolph, H. K. (1998) The medial-Golgi ion pump Pmr1 supplies the yeast secretory pathway with Ca2+ and Mn2+ required for glycosylation, sorting, and endoplasmic reticulum-associated protein degradation. *Mol. Biol. Cell* **9,** 1149–1162
12. Bolton, E. C., Mildvan, A. S., and Boeke, J. D. (2002) Inhibition of reverse transcription *in vivo* by elevated manganese ion concentration. *Mol. Cell* **9,** 879–889
13. Lue, N. F., Bosoy, D., Moriarty, T. J., Autexier, C., Altman, B., and Leng, S. (2005) Telomerase can act as a template- and RNA-independent terminal transferase. *Proc. Natl. Acad. Sci. U.S.A.* **102,** 9778–9783
14. Devasahayam, G., Ritz, D., Helliwell, S. B., Burke, D. J., and Sturgill, T. W. (2006) Pmr1, a Golgi Ca^{2+}/Mn^{2+}-ATPase, is a regulator of the target of rapamycin (TOR) signaling pathway in yeast. *Proc. Natl. Acad. Sci. U.S.A.* **103,** 17840–17845
15. Mendenhall, M. D., and Hodge, A. E. (1998) Regulation of Cdc28 cyclin-dependent protein kinase activity during the cell cycle of the yeast *Saccharomyces cerevisiae*. *Microbiol. Mol. Biol. Rev.* **62,** 1191–1243
16. Bloom, J., and Cross, F. R. (2007) Multiple levels of cyclin specificity in cell-cycle control. *Nat. Rev. Mol. Cell Biol.* **8,** 149–160
17. Booher, R. N., Deshaies, R. J., and Kirschner, M. W. (1993) Properties of *Saccharomyces cerevisiae* wee1 and its differential regulation of p34CDC28 in response to G1 and G2 cyclins. *EMBO J.* **12,** 3417–3426
18. Hu, F., and Aparicio, O. M. (2005) Swe1 regulation and transcriptional control restrict the activity of mitotic cyclins toward replication proteins in *Saccharomyces cerevisiae*. *Proc. Natl. Acad. Sci. U.S.A.* **102,** 8910–8915
19. Lew, D. J., and Reed, S. I. (1995) A cell cycle checkpoint monitors cell morphogenesis in budding yeast. *J. Cell Biol.* **129,** 739–749
20. McNulty, J. J., and Lew, D. J. (2005) Swe1p responds to cytoskeletal perturbation, not bud size, in *S. cerevisiae*. *Curr. Biol.* **15,** 2190–2198
21. Harvey, S. L., and Kellogg, D. R. (2003) Conservation of mechanisms controlling entry into mitosis: budding yeast wee1 delays entry into mitosis and is required for cell size control. *Curr. Biol.* **13,** 264–275
22. Loukin, S., and Kung, C. (1995) Manganese effectively supports yeast cell-cycle progression in place of calcium. *J. Cell Biol.* **131,** 1025–1037

23. Paidhungat, M., and Garrett, S. (1998) Cdc1 is required for growth and Mn^{2+} regulation in *Saccharomyces cerevisiae*. *Genetics* **148,** 1777–1786
24. Losev, E., Papanikou, E., Rossanese, O. W., and Glick, B. S. (2008) Cdc1p is an endoplasmic reticulum-localized putative lipid phosphatase that affects Golgi inheritance and actin polarization by activating Ca^{2+} signaling. *Mol. Cell Biol.* **28,** 3336–3343
25. Zewail, A., Xie, M. W., Xing, Y., Lin, L., Zhang, P. F., Zou, W., Saxe, J. P., and Huang, J. (2003) Novel functions of the phosphatidylinositol metabolic pathway discovered by a chemical genomics screen with wortmannin. *Proc. Natl. Acad. Sci. U.S.A.* **100,** 3345–3350
26. Pan, X., Ye, P., Yuan, D. S., Wang, X., Bader, J. S., and Boeke, J. D. (2006) A DNA integrity network in the yeast *Saccharomyces cerevisiae*. *Cell* **124,** 1069–1081
27. Suter, B., Tong, A., Chang, M., Yu, L., Brown, G. W., Boone, C., and Rine, J. (2004) The origin recognition complex links replication, sister chromatid cohesion and transcriptional silencing in *Saccharomyces cerevisiae*. *Genetics* **167,** 579–591
28. Longtine, M. S., McKenzie, A., 3rd, Demarini, D. J., Shah, N. G., Wach, A., Brachat, A., Philippsen, P., and Pringle, J. R. (1998) Additional modules for versatile and economical PCR-based gene deletion and modification in *Saccharomyces cerevisiae*. *Yeast* **14,** 953–961
29. Storici, F., and Resnick, M. A. (2006) The delitto perfetto approach to in vivo site-directed mutagenesis and chromosome rearrangements with synthetic oligonucleotides in yeast. *Methods Enzymol.* **409,** 329–345
30. Wellinger, R. E., Schär, P., and Sogo, J. M. (2003) Rad52-independent accumulation of joint circular minichromosomes during S phase in *Saccharomyces cerevisiae*. *Mol. Cell Biol.* **23,** 6363–6372
31. Foiani, M., Marini, F., Gamba, D., Lucchini, G., and Plevani, P. (1994) The B subunit of the DNA polymerase α-primase complex in *Saccharomyces cerevisiae* executes an essential function at the initial stage of DNA replication. *Mol. Cell Biol.* **14,** 923–933
32. Pellicioli, A., Lucca, C., Liberi, G., Marini, F., Lopes, M., Plevani, P., Romano, A., Di Fiore, P. P., and Foiani, M. (1999) Activation of Rad53 kinase in response to DNA damage and its effect in modulating phosphorylation of the lagging strand DNA polymerase. *EMBO J.* **18,** 6561–6572
33. Yuen, K. W., Warren, C. D., Chen, O., Kwok, T., Hieter, P., and Spencer, F. A. (2007) Systematic genome instability screens in yeast and their potential relevance to cancer. *Proc. Natl. Acad. Sci. U.S.A.* **104,** 3925–3930
34. Valerio-Santiago, M., and Monje-Casas, F. (2011) Tem1 localization to the spindle pole bodies is essential for mitotic exit and impairs spindle checkpoint function. *J. Cell Biol.* **192,** 599–614
35. Monje-Casas, F., and Amon, A. (2009) Cell polarity determinants establish asymmetry in MEN signaling. *Dev. Cell* **16,** 132–145
36. Pringle, J. R. (1991) Staining of bud scars and other cell wall chitin with calcofluor. *Methods Enzymol.* **194,** 732–735
37. Cope, M. J., Yang, S., Shang, C., and Drubin, D. G. (1999) Novel protein kinases Ark1p and Prk1p associate with and regulate the cortical actin cytoskeleton in budding yeast. *J. Cell Biol.* **144,** 1203–1218
38. Lippincott, J., and Li, R. (1998) Dual function of Cyk2, a cdc15/PSTPIP family protein, in regulating actomyosin ring dynamics and septin distribution. *J. Cell Biol.* **143,** 1947–1960
39. Santocanale, C., and Diffley, J. F. (1998) A Mec1- and Rad53-dependent checkpoint controls late-firing origins of DNA replication. *Nature* **395,** 615–618
40. Pittman, J. K., Cheng, N. H., Shigaki, T., Kunta, M., and Hirschi, K. D. (2004) Functional dependence on calcineurin by variants of the *Saccharomyces cerevisiae* vacuolar Ca^{2+}/H^{+} exchanger Vcx1p. *Mol. Microbiol.* **54,** 1104–1116
41. Lin, S. J., and Culotta, V. C. (1996) Suppression of oxidative damage by *Saccharomyces cerevisiae* ATX2, which encodes a manganese-trafficking protein that localizes to Golgi-like vesicles. *Mol. Cell Biol.* **16,** 6303–6312
42. Reddi, A. R., Jensen, L. T., Naranuntarat, A., Rosenfeld, L., Leung, E., Shah, R., and Culotta, V. C. (2009) The overlapping roles of manganese and Cu/Zn SOD in oxidative stress protection. *Free Radical Biology Medicine* **46,** 154–162
43. Lopes, M., Cotta-Ramusino, C., Pellicioli, A., Liberi, G., Plevani, P., Muzi-Falconi, M., Newlon, C. S., and Foiani, M. (2001) The DNA replication checkpoint response stabilizes stalled replication forks. *Nature* **412,** 557–561
44. Schwob, E., and Nasmyth, K. (1993) CLB5 and CLB6, a new pair of B cyclins involved in DNA replication in *Saccharomyces cerevisiae*. *Genes Dev.* **7,** 1160–1175
45. Donaldson, A. D., Raghuraman, M. K., Friedman, K. L., Cross, F. R., Brewer, B. J., and Fangman, W. L. (1998) CLB5-dependent activation of late replication origins in *S. cerevisiae*. *Mol. Cell* **2,** 173–182
46. Lisby, M., Rothstein, R., and Mortensen, U. H. (2001) Rad52 forms DNA repair and recombination centers during S phase. *Proc. Natl. Acad. Sci. U.S.A.* **98,** 8276–8282
47. Zou, J., Friesen, H., Larson, J., Huang, D., Cox, M., Tatchell, K., and Andrews, B. (2009) Regulation of cell polarity through phosphorylation of Bni4 by Pho85 G1 cyclin-dependent kinases in *Saccharomyces cerevisiae*. *Mol. Biol. Cell* **20,** 3239–3250
48. Desany, B. A., Alcasabas, A. A., Bachant, J. B., and Elledge, S. J. (1998) Recovery from DNA replicational stress is the essential function of the S-phase checkpoint pathway. *Genes Dev.* **12,** 2956–2970
49. Lew, D. J. (2000) Cell-cycle checkpoints that ensure coordination between nuclear and cytoplasmic events in *Saccharomyces cerevisiae*. *Curr. Opin. Genet. Dev.* **10,** 47–53
50. Bartholomew, C. R., Woo, S. H., Chung, Y. S., Jones, C., and Hardy, C. F. (2001) Cdc5 interacts with the Wee1 kinase in budding yeast. *Mol. Cell Biol.* **21,** 4949–4959
51. Jordan, P. W., Klein, F., and Leach, D. R. (2007) Novel roles for selected genes in meiotic DNA processing. *PLoS Genetics* **3,** e222
52. Rice, L. M., Plakas, C., and Nickels, J. T., Jr. (2005) Loss of meiotic rereplication block in *Saccharomyces cerevisiae* cells defective in Cdc28p regulation. *Eukaryot. Cell* **4,** 55–62
53. Rayner, J. C., and Munro, S. (1998) Identification of the MNN2 and MNN5 mannosyltransferases required for forming and extending the mannose branches of the outer chain mannans of *Saccharomyces cerevisiae*. *J. Biol. Chem.* **273,** 26836–26843
54. Wiggins, C. A., and Munro, S. (1998) Activity of the yeast MNN1 α-1,3-mannosyltransferase requires a motif conserved in many other families of glycosyltransferases. *Proc. Natl. Acad. Sci. U.S.A.* **95,** 7945–7950
55. Kaufman, R. J., Swaroop, M., and Murtha-Riel, P. (1994) Depletion of manganese within the secretory pathway inhibits *O*-linked glycosylation in mammalian cells. *Biochemistry* **33,** 9813–9819
56. Mondésert, G., and Reed, S. I. (1996) BED1, a gene encoding a galactosyltransferase homologue, is required for polarized growth and efficient bud emergence in *Saccharomyces cerevisiae*. *J. Cell Biol.* **132,** 137–151
57. Mondésert, G., Clarke, D. J., and Reed, S. I. (1997) Identification of genes controlling growth polarity in the budding yeast *Saccharomyces cerevisiae*: a possible role of *N*-glycosylation and involvement of the exocyst complex. *Genetics* **147,** 421–434
58. Sia, R. A., Herald, H. A., and Lew, D. J. (1996) Cdc28 tyrosine phosphorylation and the morphogenesis checkpoint in budding yeast. *Mol. Biol. Cell* **7,** 1657–1666
59. Ringvoll, J., Uldal, L., Roed, M. A., Reite, K., Baynton, K., Klungland, A., and Eide, L. (2007) Mutations in the RAD27 and SGS1 genes differentially affect the chronological and replicative lifespan of yeast cells growing on glucose and glycerol. *FEMS Yeast Res.* **7,** 848–859
60. Beckman, R. A., Mildvan, A. S., and Loeb, L. A. (1985) On the fidelity of DNA replication: manganese mutagenesis in vitro. *Biochemistry* **24,** 5810–5817
61. Jaag, H. M., Pogany, J., and Nagy, P. D. (2010) A host Ca^{2+}/Mn^{2+} ion pump is a factor in the emergence of viral RNA recombinants. *Cell Host Microbe* **7,** 74–81
62. García, R., Bermejo, C., Grau, C., Pérez, R., Rodríguez-Peña, J. M., Francois, J., Nombela, C., and Arroyo, J. (2004) The global transcriptional response to transient cell wall damage in *Saccharomyces cerevisiae* and its regulation by the cell integrity signaling pathway. *J. Biol. Chem.* **279,** 15183–15195
63. Yaakov, G., Duch, A., García-Rubio, M., Clotet, J., Jimenez, J., Aguilera, A., and Posas, F. (2009) The stress-activated protein kinase Hog1 mediates S phase delay in response to osmostress. *Mol. Biol. Cell* **20,** 3572–3582
64. Clotet, J., Escoté, X., Adrover, M. A., Yaakov, G., Garí, E., Aldea, M., de Nadal, E., and Posas, F. (2006) Phosphorylation of Hsl1 by Hog1 leads to a

G2 arrest essential for cell survival at high osmolarity. *EMBO J.* **25,** 2338–2346
65. Poletto, N. P., Henriques, J. A., and Bonatto, D. (2010) Relationship between endoplasmic reticulum- and Golgi-associated calcium homeostasis and 4-NQO-induced DNA repair in *Saccharomyces cerevisiae*. *Arch Microbiol.* **192,** 247–257
66. Zhou, Z., and Elledge, S. J. (1993) DUN1 encodes a protein kinase that controls the DNA damage response in yeast. *Cell* **75,** 1119–1127
67. Lew, D. J., and Reed, S. I. (1995) Cell cycle control of morphogenesis in budding yeast. *Curr. Opin. Genet. Dev.* **5,** 17–23
68. Kozminski, K. G., Beven, L., Angerman, E., Tong, A. H., Boone, C., and Park, H. O. (2003) Interaction between a Ras and a Rho GTPase couples selection of a growth site to the development of cell polarity in yeast. *Mol. Biol. Cell* **14,** 4958–4970
69. Ton, V. K., Mandal, D., Vahadji, C., and Rao, R. (2002) Functional expression in yeast of the human secretory pathway Ca(2+), Mn(2+)-ATPase defective in Hailey-Hailey disease. *J. Biol. Chem.* **277,** 6422–6427
70. Mohr, M. R., Erdag, G., Shada, A. L., Williams, M. E., Slingluff, C. L., Jr., and Patterson, J. W. (2011) Two patients with Hailey-Hailey disease, multiple primary melanomas, and other cancers. *Arch. Dermatol.* **147,** 211–215
71. Okunade, G. W., Miller, M. L., Azhar, M., Andringa, A., Sanford, L. P., Doetschman, T., Prasad, V., and Shull, G. E. (2007) Loss of the Atp2c1 secretory pathway Ca(2+)-ATPase (SPCA1) in mice causes Golgi stress, apoptosis, and midgestational death in homozygous embryos and squamous cell tumors in adult heterozygotes. *J. Biol. Chem.* **282,** 26517–26527